

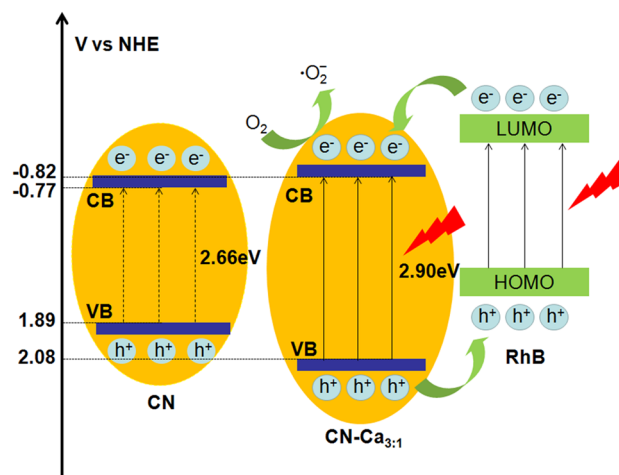
# Enhanced Photocatalysis of g-C<sub>3</sub>N<sub>4</sub> Thermally Modified with Calcium Chloride

Xiaozhou Long<sup>1,2</sup> · Tingnan Yan<sup>2</sup> · Tianjiao Hu<sup>2</sup> · Xianghui Gong<sup>2</sup> · Huaming Li<sup>1</sup> · Zengyong Chu<sup>2</sup>

Received: 27 March 2017 / Accepted: 31 May 2017 / Published online: 9 June 2017  
© Springer Science+Business Media, LLC 2017

**Abstract** Graphitic carbon nitride (g-C<sub>3</sub>N<sub>4</sub>) with improved photocatalysis was prepared via thermal polymerization of dicyandiamide with the assistance of calcium chloride. The photocatalytic activity of the modified product was optimized by changing the weight ratio of calcium chloride to dicyandiamine, and the final products were characterized by XRD, FTIR, SEM, TEM, XPS, BET, DRS and PL spectra. The results indicate that calcium chloride could lower the crystalline sizes of g-C<sub>3</sub>N<sub>4</sub> due to its coordination effect with the edge ammonia of g-C<sub>3</sub>N<sub>4</sub>. The Valence band level decreased after the modification with higher oxidation capability. The photo-generated hole and the superoxide radical are the main active species in the degradation process. As a typical performance, the degradation rate of the modified sample is more than 50 times higher than that of the un-modified carbon nitride. Due to the weakened visible light absorption of the modified catalyst, the degradation of RhB can be mainly attributed to its excitation and enhanced transfer of electrons to the catalyst.

## Graphical Abstract



**Keywords** Photocatalysis · Condensation · Crystallization · Degradation · Oxidation

## 1 Introduction

Polymeric graphitic carbon nitride (g-C<sub>3</sub>N<sub>4</sub>) is a metal free organic semiconductor and has become a hot research area in recent years due to the great application potential in pollutant degradation [1, 2], water splitting [3], CO<sub>2</sub> reduction [4] and organic synthesis [5]. g-C<sub>3</sub>N<sub>4</sub> is a layered material similar to graphite which each layer connects with others through weak van der Waals force. The elementary building blocks of g-C<sub>3</sub>N<sub>4</sub> is tri-s-triazine [6] which cross-linked by trigonal nitrogen atoms. The real material of g-C<sub>3</sub>N<sub>4</sub> consists of C, N and a small quantity of O, H. The bandgap of g-C<sub>3</sub>N<sub>4</sub> is 2.7 eV [7], its conduction band and valence band

**Electronic supplementary material** The online version of this article (doi:10.1007/s10562-017-2099-0) contains supplementary material, which is available to authorized users.

✉ Huaming Li  
lihuaming@xtu.edu.cn

✉ Zengyong Chu  
chuzy@nudt.edu.cn

<sup>1</sup> College of Chemistry, Xiangtan University,  
Xiangtan 411105, People's Republic of China

<sup>2</sup> College of Science, National University of Defense  
Technology, Changsha 410073, People's Republic of China

potentials respectively located at  $-1.1$  and  $1.6$  eV versus NHE [8].

Compared with other semiconductor catalysts, g-C<sub>3</sub>N<sub>4</sub> possess many advantages such as high thermal and chemical stability [9], low-cost, non-toxic. However, the photocatalytic activity of the bulk g-C<sub>3</sub>N<sub>4</sub> is still low due to its narrow absorption range in the visible region, high recombination rate of photogenerated electrons and holes and low specific surface area [10]. Researchs have developed various strategies to modify g-C<sub>3</sub>N<sub>4</sub> such as doping with other elements like S [11], P [12], B [13] and Br [14] to narrow its bandgap; constructing heterojunctions to promoted the separation of photoinduced electrons and holes [15–18]; designing nanostructures to increase its specific surface area [19].

In recent years, researchers have also reported on the work related to the modification of g-C<sub>3</sub>N<sub>4</sub> with alkali metal salts. Wirnhier et al. [20] obtained 2D carbon nitride through co-heating dicyandiamide and a eutectic mixture of LiCl and KCl. Yuan et al. [21] modified the texture and morphology of g-C<sub>3</sub>N<sub>4</sub> by using NaCl crystals as template. Zhang et al. [22] decreased the valence band position of g-C<sub>3</sub>N<sub>4</sub> via potassium doping using KI as potassium source.

Some researchers have also found that alkaline earth metal salts can be used as templates for the modification of graphitic carbon nitride. Wang et al. [23] obtained porous polymeric carbon nitride by using CaCO<sub>3</sub> particles as template. But their heat treatment process consists of two steps, and after the first heat treatment, hydrochloric acid was required to remove the CaCO<sub>3</sub> template.

In the present work, we develop a facile one-step co-treatment strategy to obtain modified g-C<sub>3</sub>N<sub>4</sub> using dicyandiamide (C<sub>2</sub>H<sub>4</sub>N<sub>4</sub>, DCDA) as monomers and anhydrous calcium chloride (CaCl<sub>2</sub>) as catalysts. CaCl<sub>2</sub> could react with NH<sub>3</sub> and form CaCl<sub>2</sub>·8NH<sub>3</sub> compounds and so it could influence the thermal condensation process of DCDA. In addition, CaCl<sub>2</sub> is soluble in water high solubility, making it easy to be removed from the mixture. The as-obtained modified g-C<sub>3</sub>N<sub>4</sub> (here, named as CN-Ca<sub>x</sub> for simplicity) is applied for photocatalytic RhB degradation reaction under visible light irradiation. Un-modified g-C<sub>3</sub>N<sub>4</sub>, denoted as CN here, was similarly prepared as a blank comparison. The results indicate that the photocatalytic activity was efficiently promoted after the modification.

## 2 Experimental

### 2.1 Materials

Analytical grade calcium chloride (CaCl<sub>2</sub>) was purchased from Feng Chuan Chemical Reagent Co., Ltd. Chemical purity grade dicyandiamide (DCDA) was purchased from

Sinopharm Chemical Reagent Co., Ltd. Calcium chloride was ground into powder before use and dicyandiamide was used without further purification.

### 2.2 Synthesis of CN (g-C<sub>3</sub>N<sub>4</sub>)

3 g DCDA was placed in a semi-closed ceramic crucible and heated to 550 °C at a heating rate of 20 °C min<sup>-1</sup>; then heated at 550 °C in air for 2 h. After cooling down to room temperature, the products were ground into powders and dried at 80 °C for 12 h. The obtained materials were denoted as CN.

### 2.3 Synthesis of CN-Ca<sub>x</sub>

The modified g-C<sub>3</sub>N<sub>4</sub> were prepared by mixing C<sub>2</sub>H<sub>4</sub>N<sub>4</sub> (3 g) with different amounts of CaCl<sub>2</sub> powders in mortar and ground for about 15 min, the weight ratio (CaCl<sub>2</sub>: C<sub>2</sub>H<sub>4</sub>N<sub>4</sub>) range from 1:1 to 5:1. The mixing powders were experienced heat treatment just like CN. After cooling down to room temperature, the products were ground into powders. The next two steps were very important. Firstly, the products were dissolved in about 500 mL deionized water and filter, then redissolved the residues and filter again, repeating for five times. Secondly, dissolving the residues in 100 mL deionized water, then placed the suspension into dialysis bag and dialyzed for a week. After the dialysis, the suspension orderly experienced filtration, drying, grind to obtain the final products. According to the weight ratio of calcium chloride to dicyandiamide (1:1,2:1,3:1,4:1,5:1), the products were denoted as CN-Ca<sub>1:1</sub>, CN-Ca<sub>2:1</sub>, CN-Ca<sub>3:1</sub>, CN-Ca<sub>4:1</sub> and CN-Ca<sub>5:1</sub>, respectively.

### 2.4 Characterizations

The crystal structure of the samples was characterized by Bruker Axs D8 Advance X-ray diffractometer (XRD) with Cu-K $\alpha$  ( $\lambda = 1.5406$  Å) radiation. The chemical structure of the samples was characterized by PerkinElmer double spectrum Fourier transform infrared (FT-IR) spectroscopy. The surface chemical composition of the samples and the oxidation state of the elements were analyzed by ESCALAB 250 Xi X-ray photoelectron spectrometer (XPS) with a monochromatized Al K $\alpha$  line source. The surface morphology of the samples was characterized by JSM-5600LV field emission scanning electron microscope (SEM). The optical properties of the samples were analyzed by UV-Vis diffuse reflectance spectroscopy (DRS) and photoluminescence (PL) spectroscopy. The UV-Vis DRS were obtained on a U4100 UV-Vis spectrometer. BaSO<sub>4</sub> (spectral purity) was used as a reflectance standard. The band gap of the samples was fitted by the Kubelka-Munk formula. PL were

obtained by FL-3 fluorescence spectrometer under the excitation wavelength of 380 nm at room temperature. The specific surface area of the samples were obtained through BELSORP-miniII surface area and porosity analyzer.

## 2.5 Photocatalysis Toward Degradation of RhB

The photocatalytic activities of the samples were evaluated by degradation of RhB under visible-light irradiation in a photoreaction apparatus. The apparatus consists of 350 W Xe lamp, magnetic stirrer and cooling water system. To ensure the visible-light light source, a 400 nm cut-off filter was equipped to the Xe lamp which remove light of  $\lambda < 400$  nm.

Typically, 10 mg of the photocatalysts was added into 100 mL of RhB solution with the initial concentration of  $10 \text{ mg L}^{-1}$ . The photodegradation reaction of RhB is a first-order reaction, and its degradation rate constant can be obtained according to the following equation:

$$\ln(C_t/C_0) = -kt \quad (1)$$

where  $C_0$  is the concentration of RhB solution when the catalyst and RhB reach the equilibrium of adsorption,  $C_t$  is the concentration of RhB solution at time  $t$ , and  $k$  is kinetic constant.

## 3 Results and Discussion

### 3.1 Crystallization Properties

The as-prepared samples of modified  $g\text{-C}_3\text{N}_4$  are light-white powders, not as yellow as pure carbon nitride (Supporting Information, Fig. S1–S2). The powders seem containing micrometer-sized particles (Fig. S3) or nanometer-sized particles (Fig. S4). XRD analysis of the samples were performed and are shown in Fig. 1. There are two peaks located at  $13.3^\circ$  and  $27.9^\circ$ , which can be ascribed to the (100) and (002) plane of typical graphite layer structures, respectively [24]. The peak at  $13.3^\circ$  is associated with the in-plane repeating unit of  $g\text{-C}_3\text{N}_4$  and the peak at  $27.9^\circ$  is attributed to the graphitized layered stack [7]. However, XRD patterns of  $\text{CN-Ca}_x$  has significant changes with respect to CN. On the one hand, the peak attributable to the  $g\text{-C}_3\text{N}_4$  (100) plane disappeared and a weak peak appeared at about  $10^\circ$ . It is generally regarded that the formation of 100 plane is related to the formation of a planar structure by interconnection of the in-plane repeating units 3-s-triazine rings [25]. That is to say, the in-plane repeating units of  $\text{CN-Ca}_x$  failed to construct planar structures, so the modified samples here are  $g\text{-C}_3\text{N}_4$  with smaller lateral dimension. So it can be deduced that the diffraction peak at about  $10^\circ$  is caused by the linear polymer of 3-s-triazine.

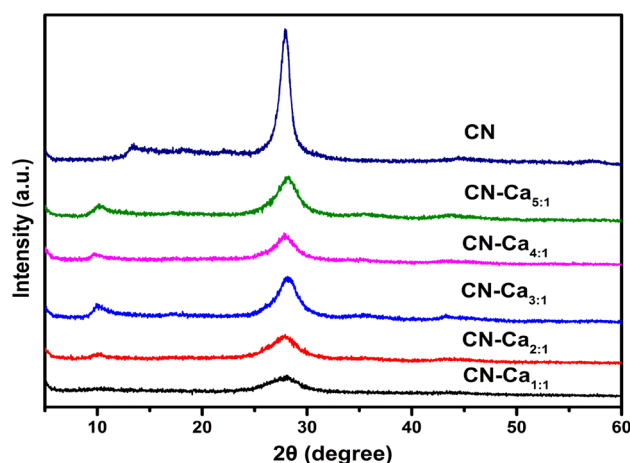


Fig. 1 XRD patterns of CN and  $\text{CN-Ca}_x$

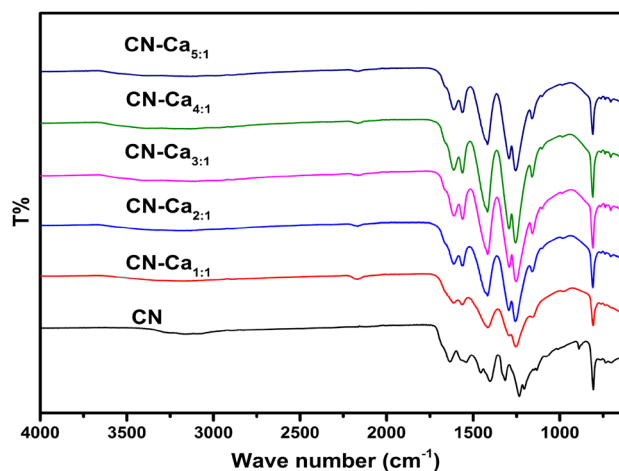


Fig. 2 FT-IR spectra of CN and  $\text{CN-Ca}_x$

On the other hand, the intensity of the peak attributable to the (002) crystal face is remarkably weakened with respect to CN, indicating a weak crystallization state of  $\text{CN-Ca}_x$ . So it can be inferred that calcium chloride could weaken the crystallization of  $g\text{-C}_3\text{N}_4$ .

### 3.2 Chemical Bonding States

FT-IR spectra of the samples were carried out and are shown in Fig. 2. As a comparison, FT-IR spectrum of  $\text{CaCl}_2$  is shown in Supporting Information, Fig. S5. The curves of CN and  $\text{CN-Ca}_x$  are very similar, which confirm that the modification does not significantly affect the chemical structure of  $g\text{-C}_3\text{N}_4$ . The peak at around  $810 \text{ cm}^{-1}$  is assigned to characteristic breathing vibration mode of triazine units [26]. The peaks at  $1200\text{--}1600 \text{ cm}^{-1}$  are ascribed to the typical stretching vibration modes of

aromatic CN heterocycles [27]. The weak and broad peak at 2850–3450 cm<sup>-1</sup> belongs to the stretching vibration of N–H and O–H bonds. However there are also some differences between the spectra of CN and CN-Ca<sub>x</sub>. The absorption peak of the characteristic breathing vibration model of 3-s-triazine in the FTIR spectra of CN-Ca<sub>x</sub> is red shifted by 2–3 cm<sup>-1</sup> compared with CN. A new peak located at 2160 cm<sup>-1</sup> emerged for CN-Ca<sub>x</sub>. As indicated in Fig. S5, the new peak belongs to the residual CaCl<sub>2</sub> in CN-Ca<sub>x</sub>. In addition, an absorption peak at 890 cm<sup>-1</sup> was observed in the FTIR spectra of CN, which is absent in CN-Ca<sub>x</sub>.

Figure 3 shows the XPS spectra of CN and CN-Ca<sub>3:1</sub>. In Fig. 3a, the weak peak at ~284.6 eV in the C 1s spectrum of CN is attributed to graphitic carbon [28], while the strong peak at ~288.1 eV is assigned to the sp<sup>2</sup>-bonded carbon atoms in the aromatic CN heterocycle (N=C=N) [29]. Comparing the C 1s spectra of CN and CN-Ca<sub>3:1</sub>, we can see that the strong peak in the C 1s spectrum of CN-Ca<sub>3:1</sub> shifts 0.2 eV to larger binding energy. The N 1s spectra of CN in Fig. 3b could be deconvoluted to four peaks, located at ~398.6, 399.8, 400.9 and 404.2 eV. These four peaks are corresponding to the sp<sup>2</sup> hybrid nitrogen (C–N=C), the tertiary nitrogen (N–(C)<sub>3</sub>) [30], the unpolymersed amino group (C–N–H) [31] on the surface and the charge effect in the heterocyclic ring [24], respectively. In Fig. 3b, it can be seen that there is a significant difference between the N 1s spectra

of CN and CN-Ca<sub>3:1</sub>. The intensity ratio of the two peaks which representative the unpolymersed amino group (C–N–H) and the tertiary nitrogen (N–(C)<sub>3</sub>) was 1.1:1 in CN, however the ratio increases to 4.1:1 for CN-Ca<sub>3:1</sub>. It means that sp<sup>3</sup>-hybrid nitrogen atoms in the form of “C–N–H” in CN-Ca<sub>3:1</sub> is remarkably increased. Based on this point, we illustrated the thermal polymerization process in Fig. 4 to show the coordination effect of CaCl<sub>2</sub>. Figure 4a is the general thermal condensation of DCDA via evolution of ammonia and Fig. 4b presents illustration of the limit-sized g-C<sub>3</sub>N<sub>4</sub> with edge-ammonia coordinated to CaCl<sub>2</sub>. We think CaCl<sub>2</sub> could promote DCDA from polymerizing into larger blocks as a salt wall, and more importantly, CaCl<sub>2</sub> could coordinate with edge-located ammonia and help to maintain more unpolymersed amino groups (C–N–H) in the modified samples. So the modified samples has weaker crystallization degrees, in agreement with the above XRD analysis. Even though the crystalline sizes seem smaller than CN, the BET surface areas of CN-Ca<sub>x</sub> did not offer any increase trend (Fig. S6), probably due to the agglomeration of micro/nano-sized particles during the common drying process. Some residue Ca<sup>2+</sup> ions were observed from XPS elemental analysis (Table S1) and due to the existence of the salt ions, the thermal stabilities of the modified samples are relatively lower than that of CN (Fig. S7).

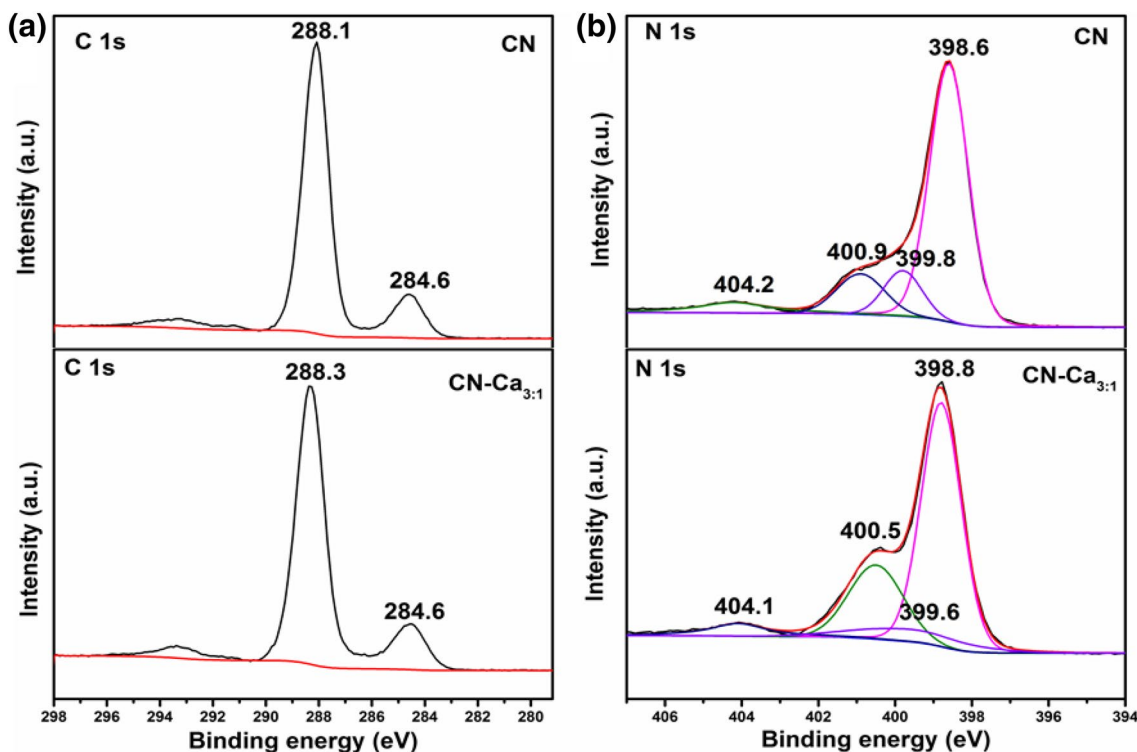
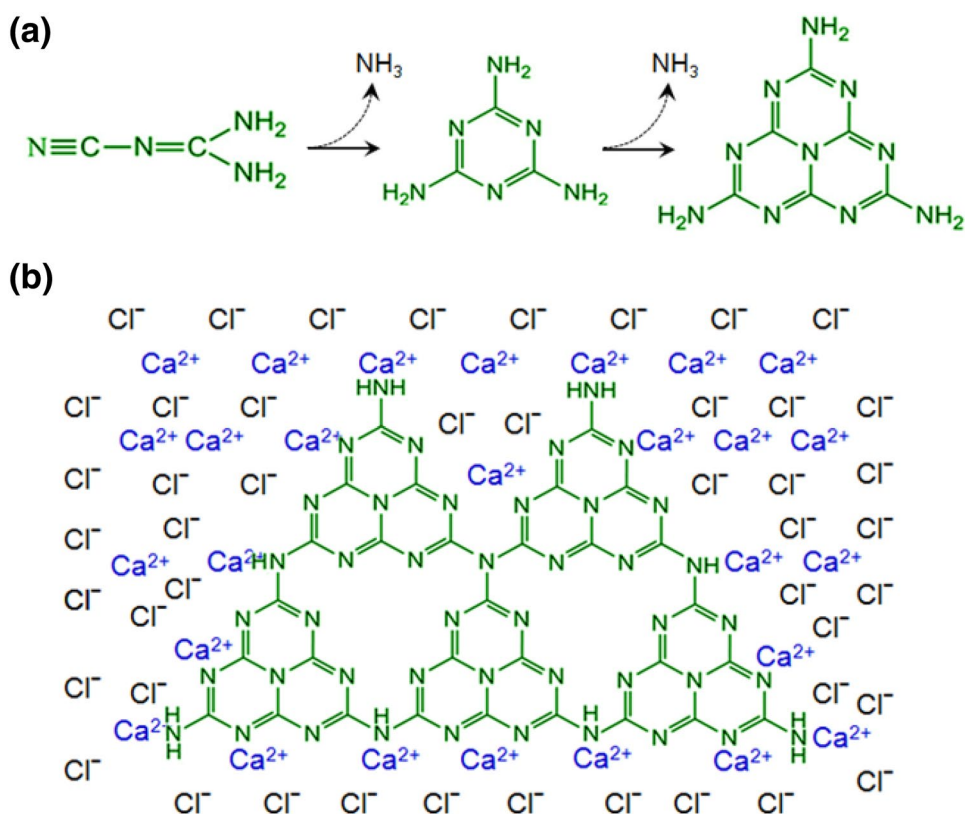


**Fig. 3** XPS spectra of CN and CN-Ca<sub>3:1</sub>. **a** C 1s spectra and **b** N 1s spectra

**Fig. 4** Thermal condensation of DCDA with the assistance of  $\text{CaCl}_2$ . **a** Reaction procedure and **b** limit-sized g- $\text{C}_3\text{N}_4$  with edge-ammonia coordinated to  $\text{CaCl}_2$



### 3.3 Optical Properties

The optical properties of the samples were analyzed using DRS and PL. The DRS spectra of CN and CN- $\text{Ca}_x$  are shown in Fig. 5a. The absorption edge of CN is located at 460 nm. However, the optical absorption edge of CN- $\text{Ca}_x$  has a significant blue shift with respect to CN. The band gaps of the samples calculated from DRS are shown in Fig. 5b. There is an increase of the band gap of CN- $\text{Ca}_x$  (0.20 eV) with respect to CN (2.66 eV). However, a decrease of the VB (0.19 eV) was observed for CN- $\text{Ca}_{3:1}$ , as shown in Fig. 5c. The room temperature PL spectra are shown in Fig. 5d. The PL intensities of CN were plotted with ten times higher but still much lower than the intensities of CN- $\text{Ca}_x$ . The maximum emission peak of CN is located at 462 nm, while the peaks are located at 441 nm for CN- $\text{Ca}_{1:1}$  and CN- $\text{Ca}_{3:1}$ . An obvious blue-shift of the emission peak to 428 nm was observed for CN- $\text{Ca}_{2:1}$ . The blue shift of absorption edge can be ascribed to the weakening of the  $\pi$ -conjugated system [32], which was consistent with the previous analysis.

### 3.4 Photocatalytic Activities

The RhB concentration evolution curves of the photocatalysts are given in Fig. 6a. Original absorption data and optical images of the degraded samples are shown in Fig.

S9–S10. The adsorption of RhB by CN- $\text{Ca}_{3:1}$  in the dark and direct photolysis of RhB serves as a control experiment. As shown, RhB did not degrade in visible light without the photocatalyst and the dark adsorption equilibrium state was reached in 30 min. Less than 10% of RhB was degraded using CN as catalyst after 90 min irradiation, while more than 90% of RhB was removed using CN- $\text{Ca}_{3:1}$  or CN- $\text{Ca}_{5:1}$ .

Straight lines in Fig. 6b confirmed the first-order reaction of the reaction and the calculated photocatalytic degradation rate constants,  $k$ , are shown in Fig. 6c. The photocatalytic degradation rates of CN- $\text{Ca}_{3:1}$  and CN- $\text{Ca}_{5:1}$  have an obviously increase with respect to CN, about 55 and 63 times higher than that of CN, respectively. Since the recycle stability of the photocatalyst is very important for its practical application, we performed stability tests using CN- $\text{Ca}_{3:1}$  as the selected photocatalyst and the results are shown in Fig. 6d and Fig. S11–S12. The photocatalytic degradation efficiency remains relatively stable after recycle for five times, indicating a good stability of CN- $\text{Ca}_x$ . It is worth noting that the photocatalytic degradation rates of CN- $\text{Ca}_{3:1}$ , CN- $\text{Ca}_{4:1}$  and CN- $\text{Ca}_{5:1}$  toward RhB are very close, no matter dialysis was applied or not. The degradation rate constant of CN- $\text{Ca}_{5:1}$  is the highest, but CN- $\text{Ca}_{3:1}$  has the comparable performance with the advantages of cost-effective.

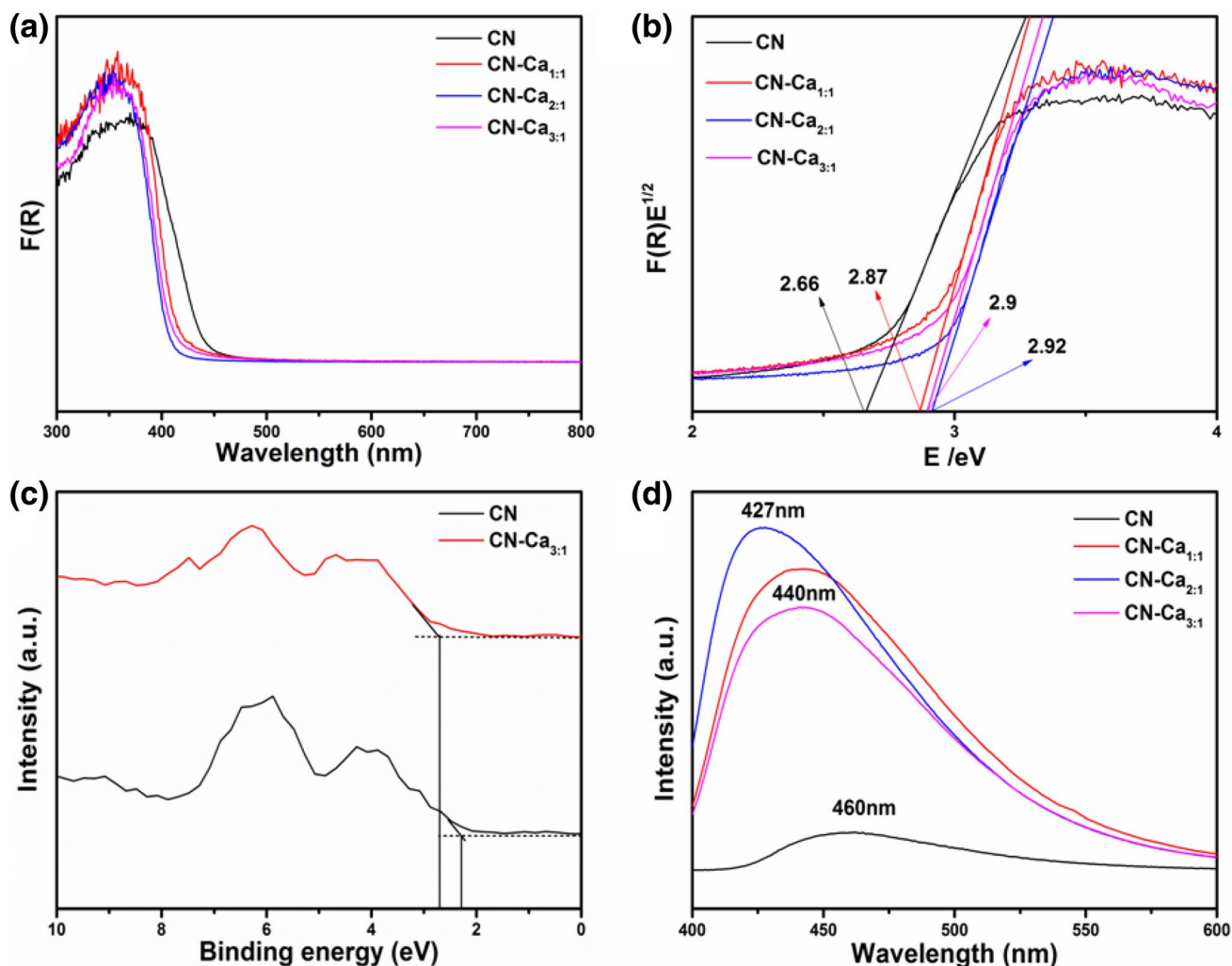


**Fig. 5** Optical properties of CN and CN-Ca<sub>x</sub>. **a** UV-Vis DRS spectra, **b** band gap spectra, **c** XPS valence band spectra, and **d** room temperature PL spectra

In general, photocatalyst will capture photons and produce four active species, namely hydroxyl radical ( $\cdot\text{OH}$ ), superoxide radical ( $\cdot\text{O}_2^-$ ), electron ( $e^-$ ) and hole ( $h^+$ ). Isopropanol (IPA), benzoquinone (BQ) and triethanolamine (TEOA) are effective scavengers of hydroxyl radical, superoxide radical and hole, respectively [33]. Therefore, IPA, BQ and TEOA can be added to the reaction system respectively to verify the main active species. As shown in Fig. 7a, 75% RhB was degraded after 60 min light irradiation in the absence of scavengers; however, only 58, 24, 7% RhB was degraded in the presence of IPA, TEOA, BQ, respectively. So it confirms that  $\cdot\text{O}_2^-$  and  $h^+$  are the main active species in the photocatalytic reaction. Hydroxyl radical is also involved in the degradation process, but its contribution to degradation process is negligible due to the limited amount. The degradation rate of RhB increases significantly when  $\text{H}_2\text{O}_2$  is

added. No degradation of RhB was observed during light irradiating the aquatic solutions of  $\text{H}_2\text{O}_2$  and dye without photocatalyst. The improved reaction activity is due to the reaction of  $\text{H}_2\text{O}_2$  and electron which produces  $\cdot\text{OH}$ . The mechanism of photocatalytic degradation of RhB is shown in Fig. 7b. On the one hand, the lowered valence band level of CN-Ca<sub>x</sub> enables the higher oxidation capability and the enhanced photocatalytic capability; on the other hand, RhB can be excited and transfer electrons to catalyst and then degrade. Due to the weakened visible light absorption of CN-Ca<sub>x</sub> above 400 nm, the latter plays a more important role. Namely, RhB molecular absorbed on the CN-Ca<sub>x</sub> catalysts generates electron-hole pairs upon visible light irradiation and transfers the excited electron to CN-Ca<sub>x</sub>, and then degrades to the transparent products with a higher oxidation state.

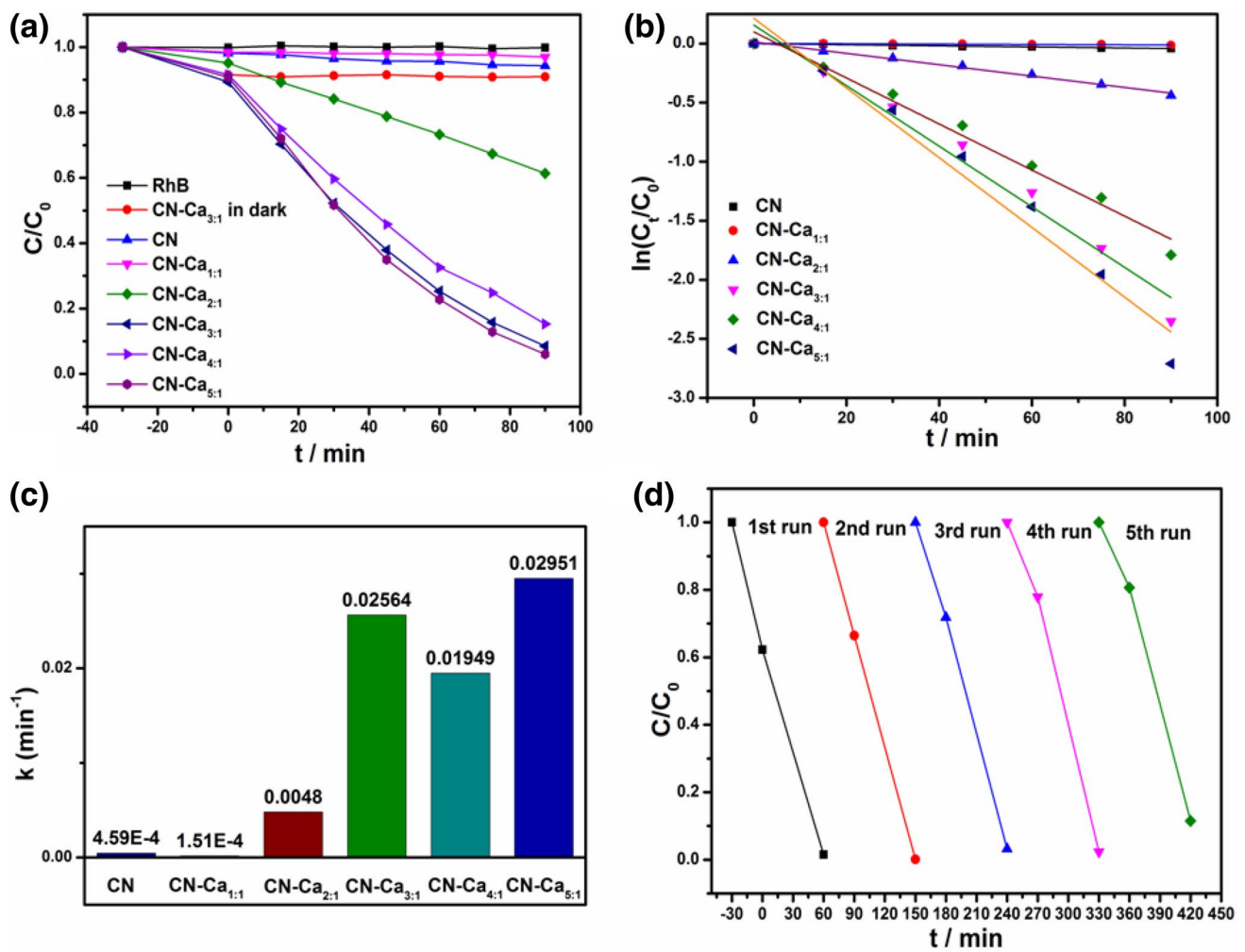


**Fig. 6** Photocatalytic activities of CN and CN-Ca<sub>x</sub>. **a** Concentration evolution curves, **b** logarithm plot, **c** degradation rate constants, and **d** recycle performance of CN-Ca<sub>3:1</sub>

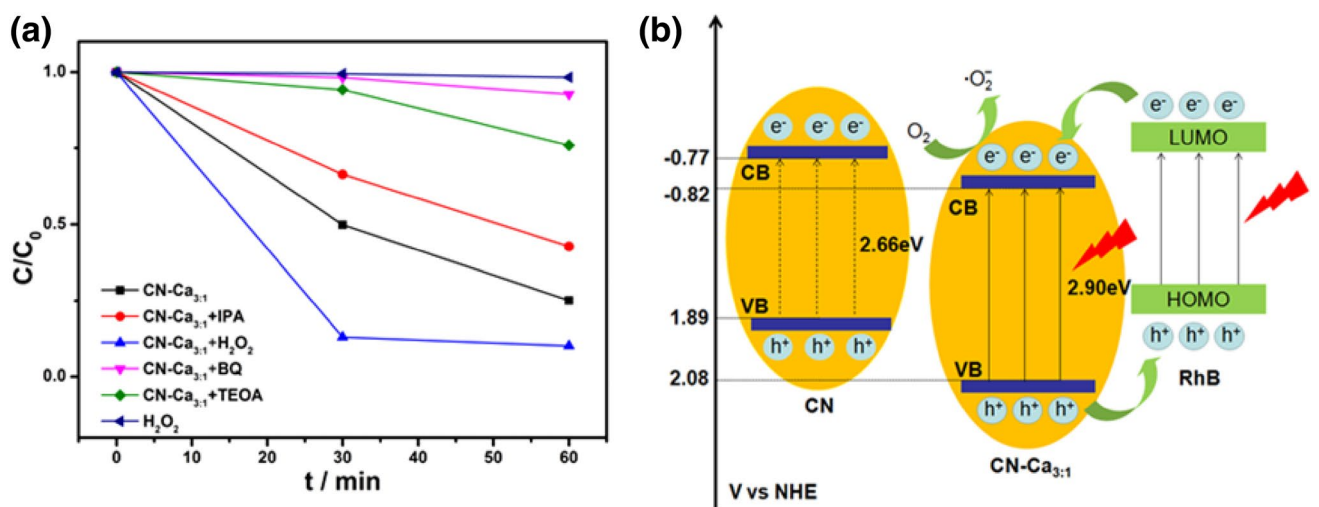


**Fig. 7** Photocatalytic mechanism analysis. **a** Photocatalytic activities in the presences of various scavengers, and **b** band structures of CN and CN-Ca<sub>3:1</sub>

## 4 Conclusion

In summary, remarkable enhancement of photocatalytic capability under visible light irradiation was achieved with the assistance of CaCl<sub>2</sub>. CaCl<sub>2</sub> could lower the crystalline sizes of g-C<sub>3</sub>N<sub>4</sub> and thus lower the valence band level of CN-Ca<sub>x</sub>, which could enhance the photocatalytic performance of CN-Ca<sub>x</sub>. The photo-generated hole and superoxide radical are the main active species in the degradation process. It is believed that the fabrication method for CN-Ca<sub>x</sub> in this work provide a new strategy to obtain g-C<sub>3</sub>N<sub>4</sub> with satisfactory photocatalysis performance.

**Acknowledgements** The whole work was carried out at National University of Defense Technology (NUDT) through a Master Joint Supervision System.

## References

- Cui Y, Ding Z, Liu P, Antonietti M, Fu X, Wang X (2012) Metal-free activation of H<sub>2</sub>O<sub>2</sub> by g-C<sub>3</sub>N<sub>4</sub> under visible light irradiation for the degradation of organic pollutants. *Phys Chem Chem Phys* 14:1455–1462
- Cheng N, Tian J, Liu Q, Ge C, Qusti AH, Asiri AM, Youbi A O A., Sun X (2013) Au-nanoparticle-loaded graphitic carbon nitride nanosheets: green photocatalytic synthesis and application toward the degradation of organic pollutants. *ACS Appl Mater Interfaces* 5:6815–6819
- Liu J, Zhang Y, Lu L, Wu G, Chen W (2012) Self-regenerated solar-driven photocatalytic water-splitting by urea derived graphitic carbon nitride with platinum nanoparticles. *Chem Commun* 48:8826–8828
- Lin J, Pan Z, Wang X (2014) Photochemical reduction of CO<sub>2</sub> by graphitic carbon nitride polymers. *ACS Sustainable Chem Eng* 2:353–358
- Wang Y, Zhang J, Wang X, Antonietti M, Li H (2010) Boron and fluorine-containing mesoporous carbon nitride polymers: metal-free catalysts for cyclohexane oxidation. *Angew Chem Int Ed* 49:3356–3359
- Kroke E, Schwarz M, Horath Bordon E, Kroll P, Noll B, Norman AD (2002) Tri-s-triazine derivatives. Part I. From trichloro-tri-s-triazine to graphitic C<sub>3</sub>N<sub>4</sub> structures Part II: alkalicymelurates M<sub>3</sub>[C<sub>6</sub>N<sub>7</sub>O<sub>3</sub>], M = Li, Na, K, Rb, Cs, manuscript in preparation. *New J Chem* 26:508–512
- Wang X, Maeda K, Thomas A, Takanabe K, Xin G, Carlsson JM, Domen K, Antonietti M (2009) A metal-free polymeric photocatalyst for hydrogen production from water under visible light. *Nat Mater* 8:76–80
- Yan SC, Lv SB, Li ZS, Zou ZG (2010) Organic-inorganic composite photocatalyst of g-C<sub>3</sub>N<sub>4</sub> and TaON with improved visible light photocatalytic activities. *Dalton Trans* 39:1488–1491
- Gillan EG (2000) Synthesis of nitrogen-rich carbon nitride networks from an energetic molecular azide precursor. *Chem Mater* 12:3906–3912
- Cao S, Low J, Yu J, Jaroniec M (2015) Polymeric photocatalysts based on graphitic carbon nitride. *Adv Mater* 27:2150–2176
- Liu G, Niu P, Sun C, Smith SC, Chen Z, Lu G, Cheng H (2010) Unique electronic structure induced high photoreactivity of sulfur-doped graphitic C<sub>3</sub>N<sub>4</sub>. *J Am Chem Soc* 132:11642–11648
- Zhang L, Chen X, Guan J, Jiang Y, Hou T, Mu X (2013) Facile synthesis of phosphorus doped graphitic carbon nitride polymers with enhanced visible-light photocatalytic activity. *Mater Res Bull* 48:3485–3491
- Yan SC, Li ZS, Zou ZG (2010) Photodegradation of rhodamine B and methyl orange over boron-doped g-C<sub>3</sub>N<sub>4</sub> under visible light irradiation. *Langmuir* 26:3894–3901
- Lan Z, Zhang G, Wang X (2016) A facile synthesis of Br-modified g-C<sub>3</sub>N<sub>4</sub> semiconductors for photoredox water splitting. *Appl Catal B* 192:116–125
- Kondo K, Murakami N, Ye C, Tsubota T, Ohno T (2013) Development of highly efficient sulfur-doped TiO<sub>2</sub> photocatalysts hybridized with graphitic carbon nitride. *Appl Catal B* 142–143:362–367
- Liu W, Wang M, Xu C, Chen S, Fu X (2013) Significantly enhanced visible-light photocatalytic activity of g-C<sub>3</sub>N<sub>4</sub> via ZnO modification and the mechanism study. *J Mol Catal A* 368–369:9–15
- Ge L, Han C, Xiao X, Guo L (2013) Synthesis and characterization of composite visible light active photocatalysts MoS<sub>2</sub>-g-C<sub>3</sub>N<sub>4</sub> with enhanced hydrogen evolution activity. *Int J Hydrogen Energy* 38:6960–6969
- Xu H, Yan J, Xu Y, Song Y, Li H, Xia J, Huang C, Wan H (2013) Novel visible-light-driven AgX/graphite-like C<sub>3</sub>N<sub>4</sub> (X = Br, I) hybrid materials with synergistic photocatalytic activity. *Appl Catal B* 129:182–193
- Xu J, Wang Y, Zhu Y (2013) Nanoporous graphitic carbon nitride with enhanced photocatalytic performance. *Langmuir* 29:10566–10572
- Wirnhier E, Doblinger M, Gunzelmann D, Senker J, Lotsch BV, Schnick W (2011) Poly(triazine imide) with intercalation of lithium and chloride ions [(C<sub>3</sub>N<sub>3</sub>)<sub>2</sub>(NH<sub>x</sub>Li<sub>1-x</sub>)<sub>3</sub>LiCl]: a crystalline 2D carbon nitride network. *Chem Eur J* 17:3213–3221
- Yuan B, Chu Z, Li G, Jiang Z, Hu T, Wang Q, Wang C (2014) Water-soluble ribbon-like graphitic carbon nitride (g-C<sub>3</sub>N<sub>4</sub>): green synthesis, self-assembly and unique optical properties. *J Mater Chem C* 2:8212–8215
- Zhang M, Bai X, Liu D, Wang J, Zhu Y (2015) Enhanced catalytic activity of potassium-doped graphitic carbon nitride induced by lower valence position. *Appl Catal B* 164:77–81
- Wang J, Zhang C, Shen Y, Zhou Z, Yu J, Li Y, Wei W, Liu S, Zhang Y (2015) Environment-friendly preparation of porous graphite-phase polymeric carbon nitride using calcium carbonate as templates, and enhanced photoelectrochemical activity. *J Mater Chem A* 3:5126–5131
- Thomas A, Fischer A, Goettmann F, Antonietti M, Müller JO, Schlögl R, Carlsson JM (2008) Graphitic carbon nitride materials: variation of structure and morphology and their use as metal-free catalysts. *J Mater Chem* 18:4893–4908
- Liu J, Zhang T, Wang Z, Dawson G, Chen W (2011) Simple pyrolysis of urea into graphitic carbon nitride with recyclable adsorption and photocatalytic activity. *J Mater Chem* 21:14398–14401
- Liao G, Chen S, Quan X, Yu H, Zhao H (2012) Graphene oxide modified g-C<sub>3</sub>N<sub>4</sub> hybrid with enhanced photocatalytic capability under visible light irradiation. *J Mater Chem* 22:2721–2726
- Liu Q, Zhang J (2013) Graphene supported Co-g-C<sub>3</sub>N<sub>4</sub> as a novel metal-macrocylic electrocatalyst for the oxygen reduction reaction in fuel cells. *Langmuir* 29:3821–3828
- Khabashesku VN, Zimmerman JL, Margrave JL (2000) Powder synthesis and characterization of amorphous carbon nitride. *Chem Mater* 12:3264–3270
- Li Y, Zhang J, Wang Q, Jin Y, Huang D, Cui Q, Zou G (2010) Nitrogen-rich carbon nitride hollow vessels: synthesis, characterization, and their properties. *J Phys Chem B* 114:9429–9434
- Guo Q, Yang Q, Zhu L, Yi C, Zhang S, Xie Y (2004) A facile one-pot solvothermal route to tubular forms of luminescent



- polymeric networks  $[(C_3N_3)_2(NH)_3]_n$ . *Solid State Commun* 132:369–374
31. Dai H, Gao X, Liu E, Yang Y, Hou W, Kang L, Fan J, Hu X (2013) Synthesis and characterization of graphitic carbon nitride sub-microspheres using microwave method under mild condition. *Diam Relat Mater* 38:109–117
  32. Ye C, Li J, Li Z, Li X, Fan X, Zhang L, Chen B, Tung C, Wu L (2015) Enhanced driving force and charge separation efficiency of protonated g- $C_3N_4$  for photocatalytic  $O_2$  evolution. *ACS Catal* 5:6973–6979
  33. Chai B, Yan J, Wang C, Ren Z, Zhu Y (2017) Enhanced visible light photocatalytic degradation of Rhodamine B over phosphorus doped graphitic carbon nitride. *Appl Surf Sci* 391:376–383